NASA
Technical
Paper
2224

October 1984

In-Flight Total Forces, Moments, and Static Aeroelastic Characteristics of an Oblique-Wing Research Airplane

Robert E. Curry
and Alex G. Sim

NASA

NASA Technical Paper 2224

1984

In-Flight Total Forces, Moments, and Static Aeroelastic Characteristics of an Oblique-Wing Research Airplane

Robert E. Curry
and Alex G. Sim

NASA Ames Research Center
Dryden Flight Research Facility
Edwards, California

National Aeronautics
and Space Administration

Scientific and Technical Information Branch

SUMMARY

A low-speed flight investigation has provided total force and moment coefficients and aeroelastic effects for the AD-1 oblique-wing research airplane. The results were interpreted and compared with predictions that were based on wind tunnel data. An assessment has been made of the aeroelastic wing bending design criteria. Lateral-directional trim requirements caused by asymmetry were determined. At angles of attack near stall, flow visualization indicated viscous flow separation and spanwise vortex flow. These effects were also apparent in the force and moment data.

INTRODUCTION

In recent years the oblique-wing configuration was proposed by Dr. R. T. Jones (ref. 1). Studies of the oblique-wing concept have shown substantially improved transonic aerodynamic performance at Mach numbers up to 1.4, and the elimination of sonic booms in flight at Mach numbers as high as 1.2 (ref. 2). Subsonic, oblique-wing transport studies have shown the potential of either increased range or increased payload (ref. 3). The anticipated low airport noise and generally better low-speed performance characteristics afforded by the unswept (high-aspect-ratio) configuration are common to both the transonic and subsonic configurations. An overview of oblique-wing technology is given in reference 4. An unmanned oblique-wing vehicle has been flight tested at sweep angles up to 45° (ref. 5). Although oblique-wing aerodynamic performance benefits occur at transonic speeds, many of the problems associated with asymmetry are not strongly tied to compressibility, and thus (to a limited extent) can be evaluated at low speeds. The AD-1 project was conducted to investigate the low-speed characteristics of an oblique-wing configuration.

The approach taken for the AD-1 project was to design and fabricate a low-speed, low-cost, airplane in which research could be conducted on many of the problems associated with an aeroelastically tailored oblique-wing airplane. The "low cost, low speed" concept limited both the complexity of the vehicle and the scope of the technical objectives. Low speed allowed the use of a simple structure, fixed landing gear, and mechanical control system. Technical objectives were limited by using only a minimal 40-channel instrumentation system. The specific technical objectives of the AD-1 program were: (1) assessment of the unique handling and flying qualities of an unaugmented, low-speed, oblique-wing vehicle; (2) general appraisal of the nature and complexity of a flight control system on an oblique-wing configuration; (3) verification of the wing static aeroelastic criteria; and (4) comparison of the flight-determined aerodynamic data with predictions.

The geometric configuration of the AD-1 aircraft was selected from airplane configurations studied by the Boeing Commercial Airplane Company under contract to NASA (ref. 2). While the overall vehicle design was specified by NASA, the detailed design and load analysis were conducted under a contracted effort by the Rutan Aircraft Factory. Fabrication was completed under a contracted effort by the Ames Industrial Corporation.

In this report, flight-determined total force and moment coefficients and aeroelastic effects are compared with preflight predictions. Based on the flight data, an evaluation of the wing static aeroelastic design criteria is made. Some characteristics of the data caused by flow separation and spanwise vortex formation at high wing sweeps and angles of attack are also identified. In conjunction with reference 6, these results provide a complete aerodynamic data package for the AD-1 research vehicle.

NOMENCLATURE

The right-hand rule is used as a basis for the force and moment sign convention. The longitudinal coefficients

are referenced to the flight stability axis, and the lateral-directional coefficients are referenced to the body axis. All data are referenced to a longitudinal center of gravity at the wing pivot (that is, 40-percent root chord), are for the right wingtip forward or at zero sweep, and include the effects of landing gear. Wing sweep is the sweep angle of the straight chord line on the wing.

a_n normal acceleration, g

a_x axial acceleration, g

a_y lateral acceleration, g

b reference and actual unswept wing span, m (ft)

c.g. center of gravity, fraction of c_r

c_r reference and unswept wing root chord, m (ft)

g acceleration due to gravity, g

I_x rolling moment of inertia, kg-m^2 (slug-ft^2)

I_{xy} x-y cross product of inertia, kg-m^2 (slug-ft^2)

I_{xz} x-z cross product of inertia, kg-m^2 (slug-ft^2)

I_y pitching moment of inertia, kg-m^2 (slug-ft^2)

I_z yawing moment of inertia, kg-m^2 (slug-ft^2)

p roll rate, deg/sec or rad/sec

q pitch rate, deg/sec or rad/sec

$\bar{q}$ dynamic pressure, N/m^2 (lb/ft^2)

r yaw rate, deg/sec or rad/sec

S reference wing area, m^2 (ft^2)

T net thrust, both engines, N (lb)

V velocity, m/sec (ft/sec)

W weight, N (lb)

WUT windup turn

α angle of attack, deg

β angle of sideslip, deg

ΔZ vertical distance from the engine thrust line to the c.g., m (ft)

δ_a aileron deflection, $\delta_{a_{left}} - \delta_{a_{right}}$, deg

δ_{a_T} aileron trim tab deflection, deg

δ_e elevator deflection, deg

δ_{e_T} elevator trim tab deflection, deg

δ_r upper rudder deflection, deg

δ_{r_T} lower rudder deflection, deg

Λ wing sweep angle, deg

ϕ bank angle, deg or rad

Coefficients:

C_D drag force

C_L lift force

C_ℓ rolling moment

C_m pitching moment

C_n yawing moment

C_Y sideforce

ΔC_ℓ rolling moment increment

ΔC_m pitching moment increment

ΔC_n yawing moment increment

Derivatives:

$$C_{m_i} = \frac{\partial C_m}{\partial i}, \text{ per deg}$$

$$C_{m_j} = \frac{\partial C_m}{\partial \frac{jC_r}{2V}}, \text{ per rad}$$

$$C_{m_k} = \frac{\partial C_m}{\partial \frac{kb}{2V}}, \text{ per rad}$$

where

$i = \alpha, \beta, \delta_a, \delta_{a_T}, \delta_e, \delta_{e_T}, \delta_r, \delta_{r_T}$

$j = q$

$k = p, r$

derivatives with respect to C_D, C_L, C_ℓ, C_n, and C_Y are of the same form as C_m.

VEHICLE DESCRIPTION AND INSTRUMENTATION

The general layout of the AD-1 airplane, shown in figure 1, consists of a high-fineness-ratio fuselage, two turbojet engines mounted on short pylons on the sides of the fuselage, fixed gear, and a high-aspect-ratio, aeroelastically tailored oblique wing. The geometric configuration is similar to that of a transonic transport design studied in reference 2. The wing can be pivoted in flight from 0° to 60° sweep, with right wing forward, and about a pivot point at the 40-percent root chord location. A total fuel capacity of 270 liters (72 gal) is stored in two fuselage tanks located forward and aft of the wing pivot location. The flight center of gravity (c.g.) was generally within a few percent of the nominal quarter root chord value. Additional physical characteristics are given in table 1. The airplane's structural composition, flight controls, and inertias are discussed in reference 6.

The wing structure was designed to deflect under aerodynamic loading to an optimum curvilinear shape at the design flight condition (lift force coefficient (C_L) = 0.3, wing sweep angle (Λ) = 60°). The actual wing deflection in bending and twist was verified before flight through static ground loading tests. The results of the loading tests are included in reference 7.

An 8-bit, 40-channel instrumentation system was used to provide flight data. Consistent with the low-cost concept, the instrumentation system was the minimum that was required to accomplish the technical objectives and ensure safety of flight. A list of instrumentation parameters relevant to the aerodynamic data analysis is presented in table 2.

WIND TUNNEL DATA

Preflight estimates of the forces and moments were obtained from wind tunnel tests of an aeroelastically scaled 1/6-scale model in NASA Ames Research Center's 12-Foot Pressure Wind Tunnel at Moffett Field, California. Full-scale Reynolds number and scaled aeroelastic wing bending were obtained while operating at 4.5 atmospheres static pressure and Mach 0.3. The wing was point designed for an optimal shape at 0.3 C_L and 60° Λ. While most of the data were obtained at these conditions, limited tests were also made at lower Mach numbers or tunnel pressures to obtain vehicle characteristics at angles of attack over 11° or at off-design wing deflections. Most of the wind tunnel data were obtained over an angle of attack range from -4° to 11°. Predictions outside this range were obtained by extrapolating the available higher angle-of-attack data. The wind tunnel data were obtained at wing sweep angles of 0°, 25°, 45°, and 60°. Predictions at 15° and 30° sweep were obtained by interpolating the wind tunnel data.

During the wind tunnel tests, two different model support configurations were used (fig. 2). In the lower sting configuration, interference with the horizontal tail flow was identified, as discussed in reference 6. Because of this interference, the upper sting configuration was used to obtain the data shown in this report. The effect of this arrangement on the vertical tail contribution is unknown, which adds some uncertainty to the drag, sideforce, yaw, and longitudinal trim predictions.

One aluminum and two fiberglass model wings were used during the wind tunnel testing. The fiberglass wings were designed to have the same scaled stiffness (in bending) as the flight vehicle structure. The aluminum wing was used for preliminary testing, but the final force, moment, and aeroelastic predictions were obtained using the more flexible fiberglass wings. The two fiberglass wings had straight 25-percent and 30-percent chord lines, respectively. Both wings had the same aspect ratio, taper ratio, and airfoil section. The straight chord line of the flight vehicle occurred at about 27-percent chord, and results from testing with the two fiberglass wings were adjusted to provide corresponding data.

It was assumed that wing bending was the primary contribution to a change in the wing shape. The wind tunnel pressure was varied to obtain changes in dynamic pressure and wing loading at constant velocity and angle of attack. The dynamic pressure necessary to cause the wing to bend to its design shape at $C_L = 0.3$ is referred to as the design dynamic pressure ($\bar{q}$) or $\bar{q}_{DESIGN}$, and most of the wind tunnel data were obtained at these conditions. Design $\bar{q}$ corresponded to 23.2 kN/m^2 (485 lb/ft^2) in the wind tunnel and 3.2 kN/m^2 (66 lb/ft^2) for the flight vehicle at 8230 N (1850 lb) gross weight. The model was photographed at the design conditions to verify that the intended wing shape was achieved.

To define the aerodynamics at off-design conditions, data were also obtained at lower dynamic pressures: $\bar{q}/\bar{q}_{DESIGN}$ values of about 0.67 and 0.40. An example of these data is shown in figure 3(a) along with extrapolated values at $\bar{q}/\bar{q}_{DESIGN}$ of 2.00 and 0 (rigid wing). In order to compare the wind tunnel data to 1g deceleration flight data, it was necessary to interpolate the wind tunnel data to a 1g fairing. The 1g fairing assumes a nominal gross weight of 8230 N (1850 lb).

It was also of interest to compare wind tunnel data to the analysis of flight windup-turn (WUT) maneuvers. WUTs are a constant $\bar{q}$ maneuver with varying angle of attack and additional loading effects. The additional loading effects have been modeled as incremental contributions to the 1g data based on load factor. The validity of this technique is discussed in appendix A. Figure 3(b) illustrates the process for determining these increments from the wind tunnel data. The design $\bar{q}$ data and the 1g fairing are plotted as a function of C_L. The increment between the two curves is shown as a function of the load factor which would occur on the flight vehicle at the same $\bar{q}/\bar{q}_{DESIGN}$ and angle of attack.

FLIGHT DATA

The flight data shown in this report were obtained during specific test maneuvers and were processed after flight by using computational techniques. Two sets of maneuvers were analyzed. Level flight decelerations (engines at idle) provided a variation of angle of attack at a constant unity load factor. Dynamic pressure and Reynolds number also varied during the decelerations. The second set of maneuvers were constant velocity windup turns that provided a variation of load factor and angle of attack at constant dynamic pressure and Reynolds number. Both sets of maneuvers

were performed slowly to avoid high angular rates and accelerations and to minimize control inputs. Trim tabs and throttle settings were not adjusted during the maneuvers. All of the data were obtained at an altitude of about 3810 m (12,500 ft). Maneuvers were analyzed at a variety of wing sweeps; however, most of the data presented in this report correspond to wing sweeps of 0°, 15°, 30°, 45°, and 60°.

RESULTS AND DISCUSSION

Force and Moment Coefficients

The six force and moment coefficients are presented as functions of angle of attack for the untrimmed airplane under 1g loading and are discussed individually.

Sideforce, rolling moment, and yawing moment are strong functions of angle of attack for the AD-1 airplane because of the oblique-wing configuration. The resultant force vector of a two-dimensional oblique wing responds primarily to the freestream flow component that is normal to the leading edge. Therefore, as angle of attack increases, the resultant vector tilts forward in the direction of the normal component and generates sideforce, roll, and yaw moments. This is generally true of an oblique-wing airplane, although some variation is expected because of three-dimensional effects.

Force and moment coefficients in 1g flight (unity load factor) were determined by solving the six equations of motion using data from the deceleration maneuvers. The complete force and moment equations used in this analysis were derived from the equations of motion given in reference 8 and are included in appendix B. Angular accelerations were estimated from angular rate data, and all data were deleted for the time interval when these accelerations became large. Sideslip, control inputs, and angular rates were accounted for by using the results of a previous flight derivative analysis (ref. 6) so that the results can be compared to the wind tunnel reference configuration. Trim tab effects were estimated in flight by balancing tab input with control input; these were included in the equations of motion. Engine thrust was estimated from ground tests and the manufacturer's specifications of altitude effects; this was also included in the equations of motion. Therefore, the force and moment coefficients that were obtained represent the untrimmed airplane in 1g steady flight with zero thrust. The moment coefficients were transferred to the reference c.g. at the wing pivot. A FORTRAN computer program was written to perform these calculations. The discrete data points from each maneuver were plotted; an example of sideforce data is shown in figure 4. Data from all maneuvers at the same conditions were combined and faired for the plots shown in this report.

Lift Coefficient

The lift coefficient results are shown in figure 5; the comparison between flight and wind tunnel is generally good. In the linear region of the data, the lift curve slopes were predicted accurately from the model data. The flight values of lift coefficients are higher than the wind tunnel results, and some differences in slope are seen at the higher angles of attack.

Nonlinearities in the lift curves (fig. 5) at high angles of attack are attributed to viscous flow separation and spanwise vortex flow. A brief flow visualization study, to be discussed in the Rolling Moment Coefficient section, supports this assumption. Flow separation, indicated by a reduction in lift curve slope and shown on the flight data of figures 5(a) to 5(e), begins at lower angles of attack than it does in the wind tunnel results. At the higher wing sweeps, lift from the formation of a spanwise vortex replaces the loss caused by separation and increases the lift curve slopes as seen in figure 5(e).

This increase in lift curve slope (vortex lift) is seen in the 45° and 60° sweep wind tunnel data but not at 45° in the flight data. Additional data from level flight decelerations at 50° and 55° sweep are shown in figure 6. In this data, evidence of vortex lift is seen at 55° and 60° sweep at angles of attack greater than 12°.

Reynolds number variation between the flight and wind tunnel tests may explain the different separated flow and spanwise vortex characteristics. Most of the wind tunnel data were obtained at a chord Reynolds number of approximately 7.5×10^6, at angles of attack (α) up to 11°. The higher α data were estimated from limited wind tunnel data at a Reynolds number of approximately 4×10^6. During the level deceleration maneuvers, the chord Reynolds number varied from 7.1×10^6 to 2.6×10^6 because of the change in airspeed. The flight data at high angles of attack were generally obtained at lower Reynolds numbers than in the wind tunnel.

As expected, the lift drops off with increasing wing sweep. This reduction may be approximated by using flight data at zero sweep and equation (1) (from two-dimensional swept wing theory).

$$C_L = C_{L_{\Lambda=0}} \cos \Lambda \qquad (1)$$

The resulting variation in lift curve slope, compared with flight data, is shown in figure 7.

Sideforce Coefficient

The wind tunnel model and flight values of sideforce coefficient are shown in figure 8. A constant bias exists between the two sets of data at all angles of attack and wing sweep, and if this bias is ignored, the comparison is good. If the wing were in the unswept position and the vehicle were symmetric, the sideforce would be zero. The flight value of sideforce coefficient at $\Lambda = 0°$ is -0.018, which indicates either a measurement bias or slight asymmetry in the airframe. Similar biases are also noted in the roll and yaw moment coefficient flight data; this implies that vehicle asymmetry is the most probable cause. Therefore, it is suggested that the bias be ignored when comparing wind tunnel and flight data.

Drag Coefficient

The drag coefficient results are shown in figure 9. Although an oblique-wing airplane would exhibit significantly lower wave drag at transonic airspeeds, the low-speed AD-1 airplane could not demonstrate this benefit. For comparison, the flight curves at 0°, 30°, and 60° sweep are shown together in figure 10. Incremental changes in drag as a function of wing sweep were observed, however. As the wing is swept, the frontal area of the airplane is reduced; this results in slightly lower profile drag. Furthermore, the aspect ratio decreases with wing sweep which results in higher induced drag.

Because performance results were not necessary to accomplish the AD-1 program objectives, precise values of drag were not demanded from this analysis. There were significant differences between the flight and wind tunnel configurations. Unlike the wind tunnel model, the flight vehicle has rounded engine inlets and some external instrumentation on the wings. There is also a larger gap between the wing and fuselage of the flight vehicle than in the wind tunnel model. While these inconsistencies are not expected to greatly affect the other force components and moments, they may have considerable impact on the profile drag force. These discrepancies suggest larger values of drag for the flight vehicle. Other error sources, such as uncertainty in the engine thrust model, may have additive or compensating effects on the flight and wind tunnel comparison.

Rolling Moment Coefficient

The general trends of the rolling moment coefficient (fig. 11) compare

favorably with wind tunnel data. Both wind tunnel and flight data indicate that the largest untrimmed roll moments at cruise angles of attack occur at about 30° sweep and decrease to virtually zero at 0° and 60° sweep. This trend is the basis of the aeroelastic design criteria and is discussed in the Aeroelastic Design Criteria section. The flight data show a constant value of 0.001 at zero sweep, which is attributed to the airplane asymmetry suggested by the sideforce data.

Because of the limited angle-of-attack range of the wind tunnel tests and variations in Reynolds number, the effects of high angle of attack were not well defined in the wind tunnel data. At 60° sweep, evidence of trailing-edge separation is seen in the flight data at angles of attack above 8°. Trailing-edge separation on the aft (left) wing results in negative rolling moments. The onset of vortex lift on the aft wing occurs at 12° angle of attack; this results in less negative rolling moments. These effects are indicated on the flight data in figure 11(e). Note that vortex lift is also observed in the lift coefficient data (fig. 5) above 12° angle of attack. At greater angles of attack, flow separation increases on the aft wing which results in rolloff to the left. Lateral control effectiveness is reduced under these conditions because of tip separation which makes it impossible to reach higher angles of attack in steady flight. Complete wing stall was not possible at 60° sweep.

A brief flow-field study was performed to verify these high-angle-of-attack effects. Tufts were attached to the upper surface of the entire wing and were photographed in flight with the wing at 60° sweep. Streamwise attached flow was indicated by the tufts on the forward (right) wing at angles of attack up to 15°. Tuft patterns observed on the aft wing, shown schematically in figure 12, show considerable separation developing by 12° angle of attack, and the spanwise vortex is well defined by 15° angle of attack. This confirms the analysis of the roll coefficient data.

Pitching Moment Coefficient

The pitching moment coefficient results (fig. 13) do not exhibit a close comparison between wind tunnel and flight data. Much of the discrepancy may be caused by an inaccurate prediction of longitudinal trim. This is a difficult term to predict from wind tunnel tests and may have been affected by sting interference (ref. 6).

Yawing Moment Coefficient

The yawing moment coefficients are shown in figure 14. The flight data show a small value at 0° sweep for all angles of attack. Again, this is caused by the asymmetry of the vehicle. Correlation between flight and wind tunnel data is poor. For cruise flight, the yawing moment is relatively small (compared to roll and pitch) and difficult to measure from the quasi-static maneuvers used in this analysis.

Aeroelastic Design Criteria

The goal of the aeroelastically tailored wing design criteria was to minimize the roll trim requirements at the design point flight conditions. In straight-and-level flight, the AD-1 airplane design conditions are 60° sweep and 0.3 lift coefficient. This corresponds to an angle of attack of about 4°. The wing was intended to deflect sufficiently under 1g load to balance the untrimmed span load about the centerline of the vehicle. The untrimmed roll coefficient (fig. 11) is near zero at 60° sweep and 4° angle of attack, indicating that the design goal has been met. At intermediate wing sweeps between 0° and 60°, significant untrimmed roll moments do exist. In order to equalize these moments at off-design wing sweeps, at most, 18 percent of the available roll control authority is required when using significant rudder trim.

Lateral-Directional Trim

Sideforce has a strong influence on the trim requirements of an oblique-wing airplane. In order to eliminate lateral motion, this sideforce must be balanced by holding bank angle or sideslip angle, or a combination of both. For steady, straight-and-level flight, the translational forces on the vehicle can be approximated with equation (2). Control inputs, drag components, and lift caused by sideslip have been neglected.

$$C_Y + C_{Y_\beta} \times \beta = -C_L \times \phi \qquad (2)$$

This trim relationship between bank and sideslip angles for the AD-1 airplane is shown in figure 15, for a lift coefficient of 0.3 at 60°. Flight values of C_{Y_β} were obtained from reference 6, and values of C_Y were obtained from figure 8.

The angle of the wing pivot axis with respect to the fuselage is an important aspect in the design of oblique-wing airplanes. If this axis is tilted forward, the wing will develop a bank angle in relation to the fuselage as it is swept. For a design flight condition, this pivot axis angle can be chosen so that the fuselage remains unbanked when the wing has attained an effective bank angle sufficient to balance the lateral forces with 0° sideslip.

The wing pivot axis of the AD-1 airplane is perpendicular to the fuselage. Figure 15 shows that for a design point of $\Lambda = 60°$ and $C_L = 0.3$, about 9.6° of bank is necessary for trim without sideslip. If the wing pivot axis had been tilted forward 5.5°, the AD-1 airplane wing would achieve this bank angle with respect to the fuselage at 60° sweep, thus eliminating the need to bank the fuselage to obtain 0° sideslip.

Load Factor Effects

The moment characteristics at load factors greater than one were determined by analyzing data obtained from windup turns at about the design $\bar{q}$. Considerable variation exists in the moment coefficients computed from windup turn data and those computed from 1g maneuvers. As an example, the pitching moment coefficients at 60° sweep are compared in figure 16. Computationally, the roll, pitch, and yaw moment coefficients at 1g were subtracted from the elevated-g values. The remainders are referred to as rolling moment increment (ΔC_ℓ), pitching moment increment (ΔC_m), and yawing moment increment (ΔC_n), and are shown in figure 17. These terms represent the increments on the moment coefficients at load factors other than unity.

In order to analyze the forces and moments under elevated-g loading it was necessary to assume that the sideslip, damping, and control derivatives do not vary with load factor. For most of the terms this was a good assumption. Possible exceptions, such as C_{ℓ_β}, may have introduced some error into the analysis. Derivative data (ref. 6) were obtained only in 1g flight because the flying characteristics made precise maneuvering under accelerated conditions difficult. Furthermore, the control derivatives were assumed to be linear throughout the range of control authority. This was probably not valid for large aileron deflections when combined with high angle of attack. This condition occurred during low-speed flight with the wing swept because large aileron deflections were often used for trim.

The incremental effects on ΔC_ℓ, ΔC_m, and ΔC_n caused by elevated g (load factors greater than unity) are presented in figure 17. These data were obtained near the design $\bar{q}$. The effects of lower dynamic pressure on these increments were studied by performing windup-turn maneuvers at various airspeeds. Biases occurred because of dynamic pressure changes; however, the slopes of the moment increments with respect to load factor did not vary significantly for

data near design $\bar{q}$. Both wind tunnel and flight tests confirmed that the force coefficients did not vary with load factor or dynamic pressure. A more detailed discussion of these characteristics is given in appendix A.

The moment increments had a significant impact on the stability of the vehicle at higher load factors. As seen in the example of figure 16, the AD-1 airplane was considerably more stable longitudinally during 1g decelerations than during elevated g windup turns (these data are for the reference c.g. only; the vehicle was never flown statically unstable). The AD-1 airplane structure was adequate to complete the technical objectives of the project; however, a stiffer wing accompanied by appropriate geometric changes would have improved the flying qualities by reducing the load factor effects.

CONCLUDING REMARKS

The total force and moment coefficients for the AD-1 oblique-wing research airplane have been obtained from flight tests. These were determined as functions of angle of attack at unity load factor. The flight results were compared with predictions based on wind tunnel model data. The correlation was generally good, although it was less favorable for the drag and yaw moment components. The data also indicated significant flow separation and spanwise vortex flow effects which were verified by flow visualization at high angles of attack.

The static aeroelastically tailored wing design criteria resulted in minimal roll trim requirements at a 60° sweep design flight condition. The bank and sideslip angles required for trim were determined for the flight vehicle. It is suggested that optimal selection of the wing pivot axis angle could eliminate this requirement on future designs.

The moment coefficient characteristics at higher load factors were also determined in flight. Longitudinal static stability was significantly reduced during elevated-g maneuvers. Increased wing stiffness would have improved the flying qualities of the airplane.

Ames Research Center
Dryden Flight Research Facility
National Aeronautics and Space Administration
Edwards, California, June 6, 1983

APPENDIX A — AEROELASTICITY MODELING

Because of the oblique-wing configuration, the AD-1 airplane demonstrates unique aeroelastic properties. These properties greatly affected the flying qualities and had to be modeled to obtain a valid simulation. Because of the limited range of test altitude and airplane gross weight, data could not be obtained only as a function of dynamic pressure without varying angle of attack. The available flight data consists of 1g decelerations, windup turns at near the design $\bar{q}$, and windup turns at lower dynamic pressures. The lower $\bar{q}$ windup-turn data is limited in quality and quantity because of poor flying qualities at high angles of attack, especially at high sweep angles. At 35° sweep a reasonable set of windup turns at various $\bar{q}/\bar{q}_{DESIGN}$ was obtained. These data are used to illustrate two features of the aeroelastic modeling presented in this paper.

The first feature is that aeroelastic effects on force data can be neglected. Generally, the aeroelastic effects on a conventional swept wing airplane result in a change in lift curve slope caused by the geometric twist associated with wing bending. For aft swept wings this results in a decrease in lift curve slope and for forward swept wings this results in an increase in lift curve slope. As shown in figure 18, the AD-1 airplane exhibits no significant change in lift curve slope during changes in dynamic pressure. This is probably caused by a canceling of the aeroelastic effects of the forward and aft swept portions of the oblique wing. The second feature is that shifting of the load centroid, caused by different aeroelastic effects of the forward and aft swept portions of the wing, results in a significant moment variation with loading. Generally, any change in wing shape because of maneuvering or airspeed changes will change the moment coefficients.

These characteristics have been presented in this report as 1g data (corresponding to level flight decelerations with varying $\bar{q}$ and α) and the incremental effect of additional loading at the design $\bar{q}$ as a function of load factor. Using this modeling technique, a satisfactory simulation of the vehicle flying qualities was possible. Airplane gross weight varied about ±10 percent around the nominal value of 8230 N (1850 lb) during flight testing and was assumed to be constant. This was necessary in order to show the incremental effects as a function of load factor.

The moment coefficients at Λ = 35° from a 1g deceleration and windup turns at the design and lower dynamic pressures are compared in figure 19. The off-design $\bar{q}$ windup-turn data generally do not intersect the 1g data and thus indicate a small moment bias (trim) error in the model. This error may be caused by power effects which were present in the windup turns. If the increments between the windup turn (WUT) and deceleration values are plotted as a function of load factor (fig. 20), the slopes of these increments with load factor are similar for values of $\bar{q}$ near design $\bar{q}$. As previously mentioned the quantity of the data at lower $\bar{q}$ (higher α) is limited and is considered to be of unsatisfactory quality to define such variations. Therefore, the set of increments obtained at the design $\bar{q}$ was used in the simulator model for all dynamic pressures. The simulation produces realistic dynamic response at all dynamic pressures although the response at low $\bar{q}$ was not rigorously evaluated. The biases which occur in the moment increments because of varying dynamic pressure result in a trim change for the flight vehicle and were not modeled in the AD-1 simulation.

APPENDIX B — UNTRIMMED FORCE AND MOMENT COEFFICIENT EQUATIONS

Force:

$$C_L = \frac{W}{\bar{q}S}\left(a_n \cos\alpha + a_x \sin\alpha\right) - \left(C_{L_\beta} \times \beta + C_{L_{\delta_a}} \times \delta_a + C_{L_{\delta_e}} \times \delta_e + \frac{b}{2V} C_{L_p} \times p + \frac{c_r}{2V} C_{L_q} \times q + \frac{b}{2V} C_{L_r} \times r\right)$$

$$C_Y = \frac{Wa_y}{\bar{q}S} - \left(C_{Y_\beta} \times \beta + C_{Y_{\delta_a}} \times \delta_a + C_{Y_{\delta_r}} \times \delta_r + C_{Y_{\delta_{r_T}}} \times \delta_{r_T} + \frac{b}{2V} C_{Y_p} \times p + \frac{C_r}{2V} C_{Y_q} \times q + \frac{b}{2V} C_{Y_r} \times r\right)$$

$$C_D = \frac{1}{\bar{q}S}\left[T \cos\alpha + W\left(a_n \sin\alpha - a_x \cos\alpha\right)\right] - \left(C_{D_\beta} \times \beta + C_{D_{\delta_a}} \times \delta_a + C_{D_{\delta_e}} \times \delta_e + C_{D_{\delta_r}} \times \delta_r + C_{D_{\delta_{r_T}}} \times \delta_{r_T}\right)$$

Moment:

$$C_\ell = \frac{1}{\bar{q}Sb}\left[qr\left(I_z - I_y\right) + prI_{xy} - pqI_{xz}\right] - \left(C_{\ell_\beta} \times \beta + C_{\ell_{\delta_a}} \times \delta_a + C_{\ell_{\delta_{a_T}}} \times \delta_{a_T} + C_{\ell_{\delta_r}} \times \delta_r + C_{\ell_{\delta_{r_T}}} \times \delta_{r_T} + \frac{b}{2V} C_{\ell_p} \times p + \frac{C_r}{2V} C_{\ell_q} \times q + \frac{b}{2V} C_{\ell_r} \times r\right)$$

$$C_m = \frac{1}{\bar{q}SC_r}\left[pr\left(I_x - I_z\right) - q_r I_{xy} - \Delta Z_T\right] - \left(C_{m_\beta} \times \beta + C_{m_{\delta_a}} \times \delta_a + C_{m_{\delta_e}} \times \delta_e + C_{m_{\delta_{e_T}}} \times \delta_{e_T} + \frac{b}{2V} C_{m_p} \times p + \frac{C_r}{2V} C_{m_q} \times q + \frac{b}{2V} C_{m_r} \times r\right)$$

$$C_n = \frac{1}{\bar{q}Sb}\left[pq\left(I_y - I_x\right) + \left(q^2 - p^2\right)I_{xy} + qrI_{xz}\right] - \left(C_{n_\beta} \times \beta + C_{n_{\delta_a}} \times \delta_a + C_{n_{\delta_r}} \times \delta_r + C_{n_{\delta_{r_T}}} \times \delta_{r_T} + \frac{b}{2V} C_{n_p} \times p + \frac{C_r}{2V} C_{n_q} \times q + \frac{b}{2V} C_{n_r} \times r\right)$$

REFERENCES

1. Jones, R. T.: New Design Goals and a New Shape for the SST. Astronaut. and Aeronaut., vol. 10, no. 12, Dec. 1972, pp. 66-70.

2. Boeing Commercial Airplane Company Preliminary Design Department: Oblique Wing Transonic Transport Configuration Development. NASA CR-151928, 1977.

3. Bradley, E. S.: Summary Report — An Analytical Study for Subsonic Oblique Wing Transport Concept. NASA CR-137897, 1976.

4. Nelms, Walter P., Jr.: Applications of Oblique-Wing Technology — An Overview. AIAA Paper 76-943, Sept. 1976.

5. Maine, Richard E.: Aerodynamic Derivatives for an Oblique Wing Aircraft Estimated From Flight Data by Using a Maximum Likelihood Technique. NASA TP-1336, 1978.

6. Sim, Alex G.; and Curry, Robert E.: Flight-Determined Aerodynamic Derivatives of the AD-1 Oblique-Wing Research Airplane. TP-2222, 1984.

7. Andrews, W. H.; Sim, A. G.; Monaghan, R. C.; Felt, L. R.; and McMurtry, T. C.: AD-1 Oblique Wing Aircraft Program. SAE Paper 801180, Oct. 1980.

8. Gainer, Thomas G.; and Hoffman, Sherwood: Summary of Transformation Equations and Equations of Motion Used in Free-Flight and Wind-Tunnel Data Reduction and Analysis. NASA SP-3070, 1972.

TABLE 1. — PHYSICAL CHARACTERISTICS OF AD-1 AIRPLANE

Total height, m (ft)	2.06 (6.75)
Total length, m (ft)	11.80 (38.80)
Wing (Λ = 0°) —	
Reference and actual planform area, m^2 (ft^2)	8.60 (93.00)
Reference and unswept span, m (ft)	9.80 (32.30)
Reference and unswept chord (root), m (ft)	1.30 (4.28)
Aspect ratio	11.2
Airfoil	NACA 3612-02, 40 (constant)
Dihedral angle, deg	0
Twist, deg	-2
Root incidence angle, deg	2
Quarter chord sweep angle, deg	0
Leading edge sweep angle, deg	2
Average chord, m (ft)	0.88 (2.90)
Wing pivot location	$0.4c_r$
Sweep angle range, deg	0 to 60
Horizontal tail —	
Planform area, m^2 (ft^2)	2.40 (26.00)
Span, m (ft)	2.40 (8.00)
Average chord, m (ft)	1.00 (3.30)
Root chord, m (ft)	1.60 (5.40)
Dihedral angle, deg	0
Incidence angle, deg	0
Leading edge sweep angle, deg	45
Airfoil	NACA 0006
Vertical tail —	
Area (exposed), m^2 (ft^2)	1.30 (14.40)
Span (exposed), m (ft)	1.10 (3.70)
Average chord, m (ft)	1.20 (3.90)
Root chord, m (ft)	1.80 (5.80)
Leading edge sweep angle, deg	43
Airfoil	NACA 0006
Primary control surfaces —	
Aileron hinge line	$0.75c_r$
Aileron span (total), m (ft)	3.70 (12.00)
Aileron area, each, m^2 (ft^2)	0.28 (3.00)
Aileron root station, $\frac{Y}{b/2}$	0.62
Aileron root chord, m (ft)	0.20 (0.65)
Aileron range, each, deg	±25
Elevator hinge line sweep angle, deg	0
Elevator area, m^2 (ft^2)	0.46 (5.00)
Elevator average chord, m (ft)	0.19 (0.62)
Elevator root chord, m (ft)	0.23 (0.75)
Elevator range, deg	25° up to 15° down
Rudder hinge line sweep angle, deg	0
Rudder area, m^2 (ft^2)	0.14 (1.51)
Rudder average chord, m (ft)	0.24 (0.77)
Rudder root chord, m (ft)	0.28 (0.91)
Rudder range, deg	±25

TABLE 1. — Concluded

Masses —

Empty weight, N (lb)	6450 (1450)
Useful load, N (lb)	2930 (695)
Fuel load, N (lb)	2110 (475)
Gross weight, N (lb)	9540 (2145)

Powerplant —

Engines	Two TRS-18-046
Sea-level static thrust, each, N (lb)	979 (220)

TABLE 2. — SELECTED INSTRUMENTATION PARAMETERS

Parameter description	Range	Accuracy
Angle of attack, deg	-5 to 20	0.5
Angle of sideslip, deg	-15 to 15	0.5
Airspeed, knots	0 to 200	3.0
Altitude, m (ft)	0 to 6100 (0 to 20,000)	90.0 (300)
Free air reference temperature, °C (°F)	-45 to 65 (-49 to 149)	2.0 (3.6)
Pitch attitude, deg	-30 to 30	0.6
Roll attitude, deg	-30 to 30	0.6
Pitch rate, deg/sec	-60 to 60	0.3
Roll rate, deg/sec	-60 to 60	0.6
Yaw rate, deg/sec	-30 to 30	0.3
Normal acceleration, g	-1 to 4	0.025
Lateral acceleration, g	-0.5 to 0.5	0.005
Longitudinal acceleration, g	-0.5 to 0.5	0.005
Wing sweep angle, deg	0 to 60	0.6
Right aileron, deg	-25 to 25	0.5
Left aileron, deg	-25 to 25	0.5
Elevator, deg	-27 to 15	0.4
Rudder, deg	-25 to 25	0.5
Right throttle, percent	60 to 110	1.0
Left throttle, percent	60 to 110	1.0
Aileron trim tab, deg	-20 to 20	0.4
Elevator trim tab, deg	-20 to 20	0.4
Rudder trim, deg	-22 to 7	0.3

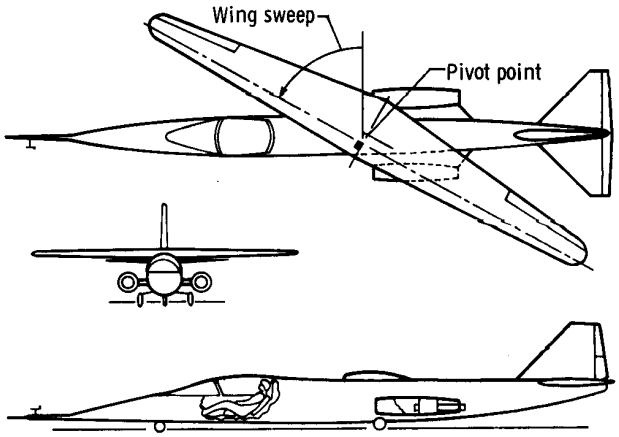

Figure 1. General configuration of the AD-1 oblique wing airplane; Λ = 60°.

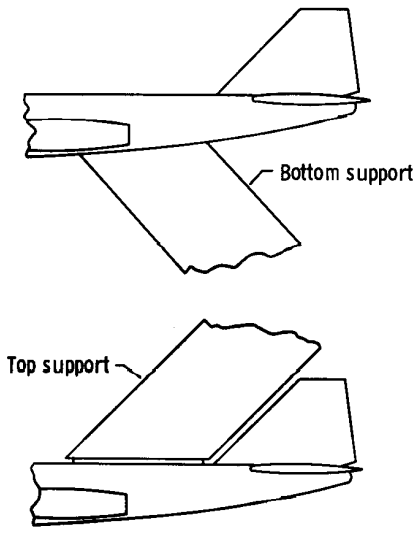

Figure 2. Wind tunnel model blade support arrangements.

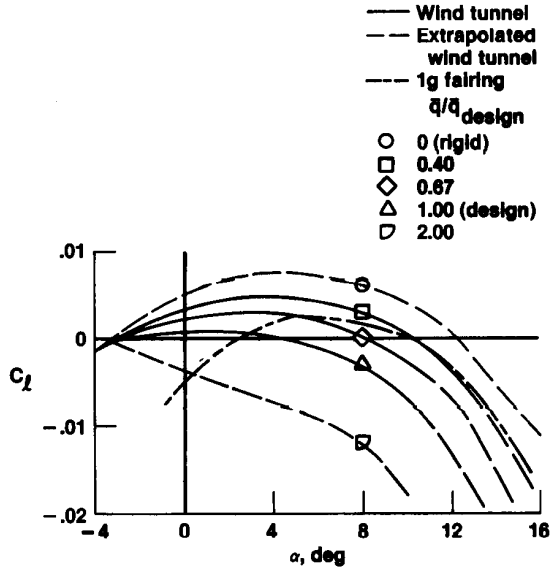

(a) lg characteristics.

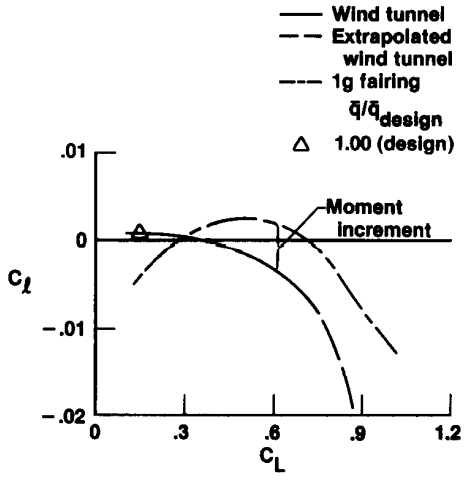

(b) Moment increment extraction.

Figure 3. Example of wind tunnel moment data reduction; Λ = 45°.

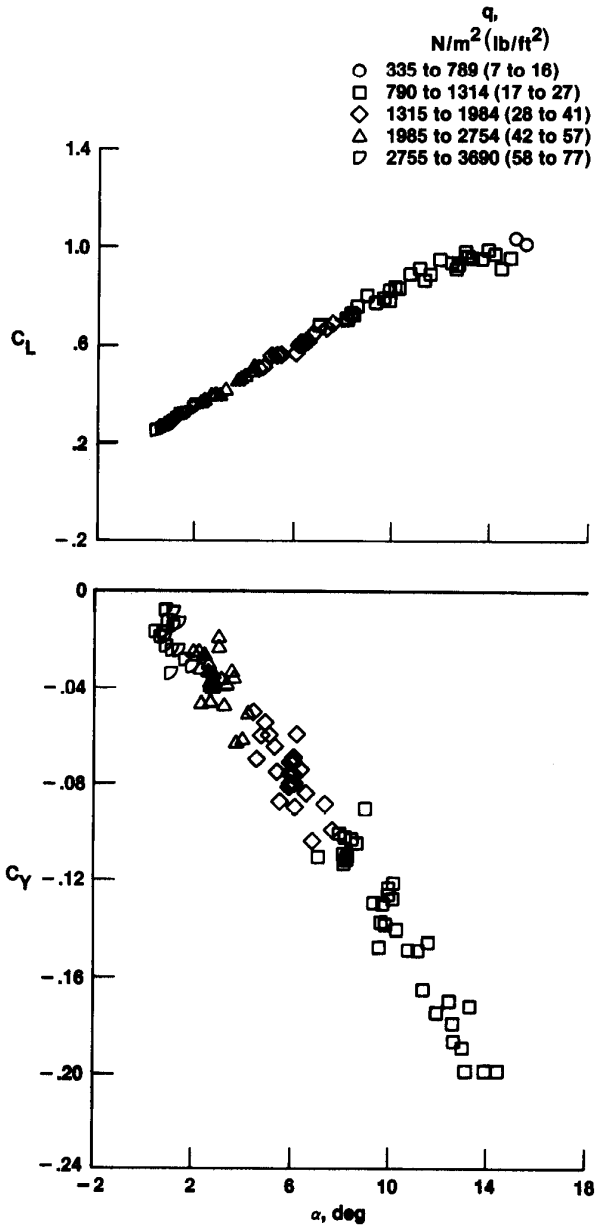

Figure 4. Example of unfaired flight sideforce data from a deceleration maneuver; Λ = 45°.

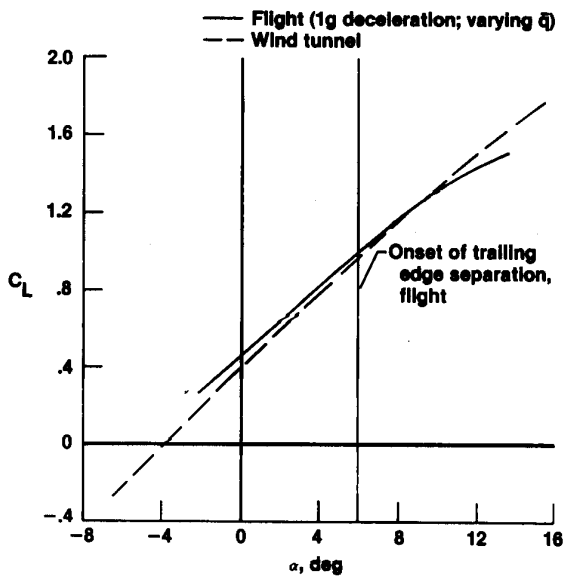

(a) Λ = 0°.

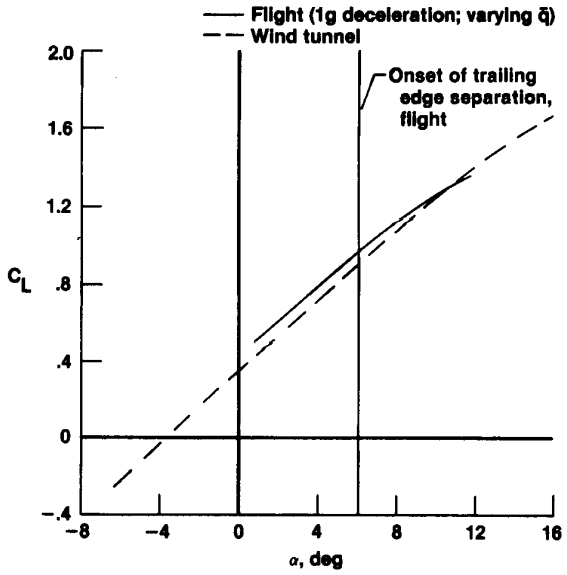

(b) Λ = 15°.

Figure 5. Untrimmed lift coefficient results.

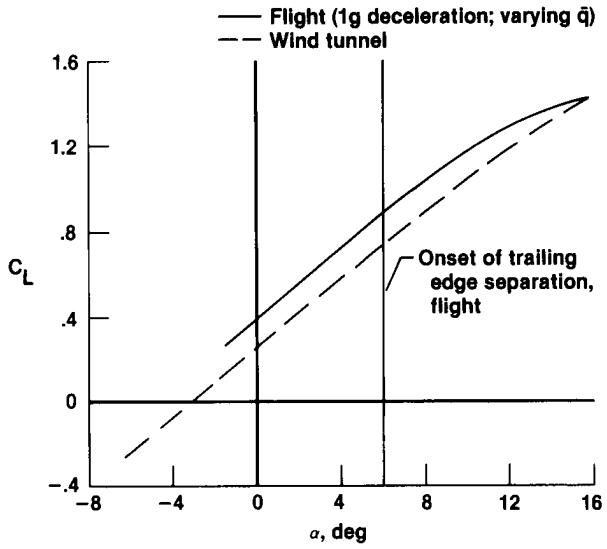

(c) $\Lambda = 30°$.

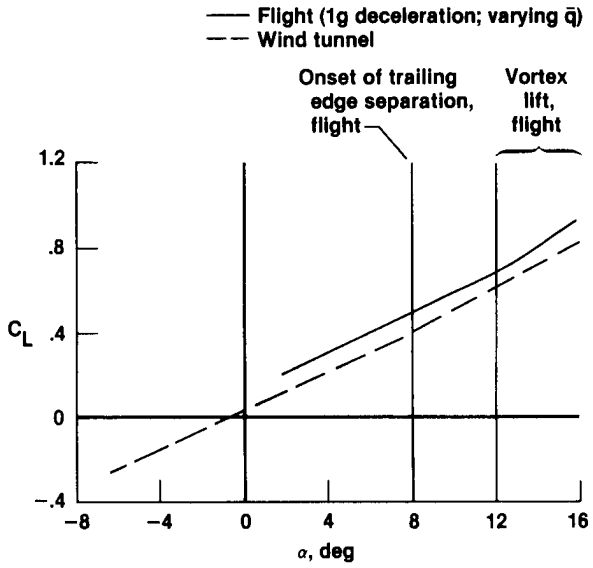

(e) $\Lambda = 60°$.

Figure 5. Concluded.

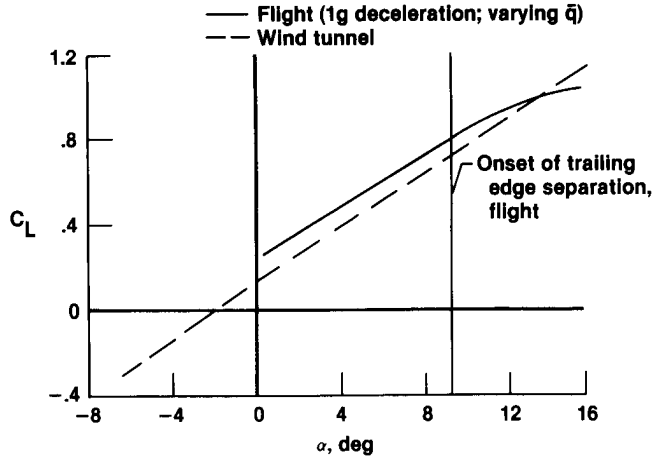

(d) $\Lambda = 45°$.

Figure 5. Continued.

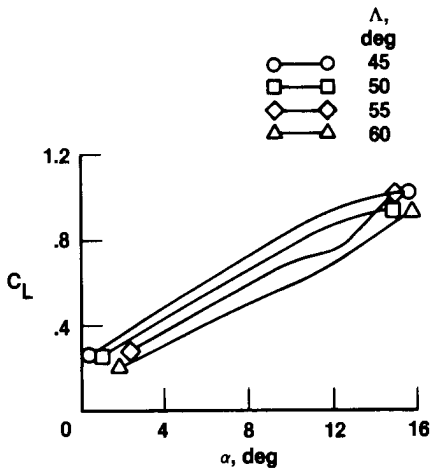

Figure 6. Untrimmed lift coefficient at high wing sweeps in flight.

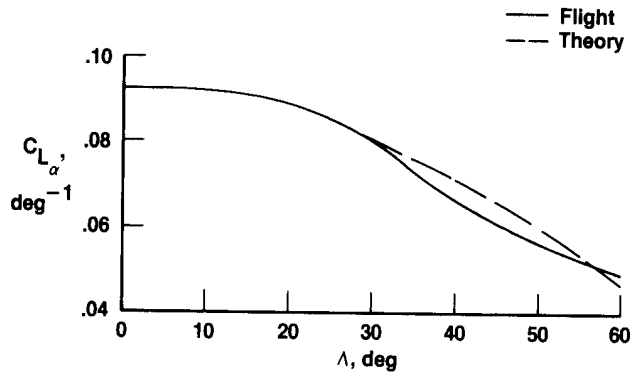

Figure 7. Variation in lift curve slope with wing sweep; α = 4°.

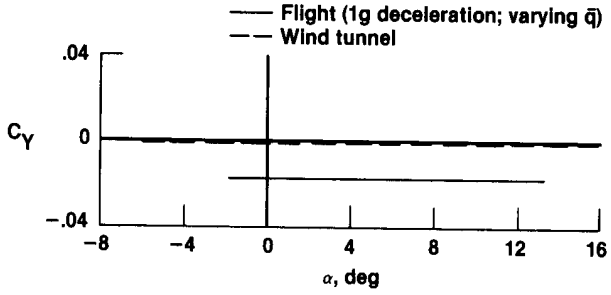

(a) Λ = 0°.

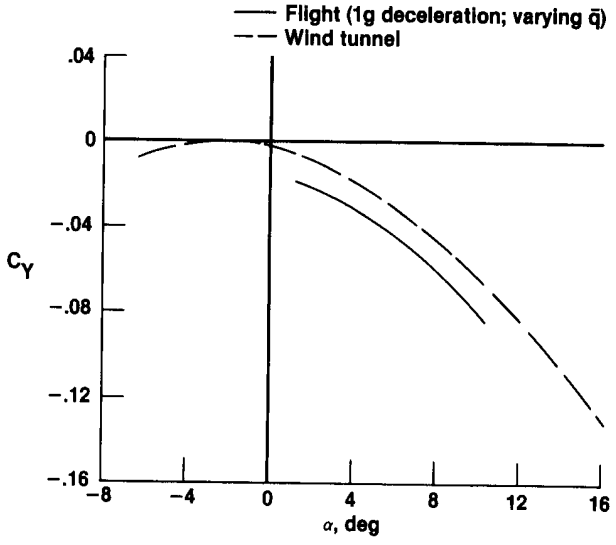

(b) Λ = 15°.

Figure 8. Untrimmed sideforce coefficient results.

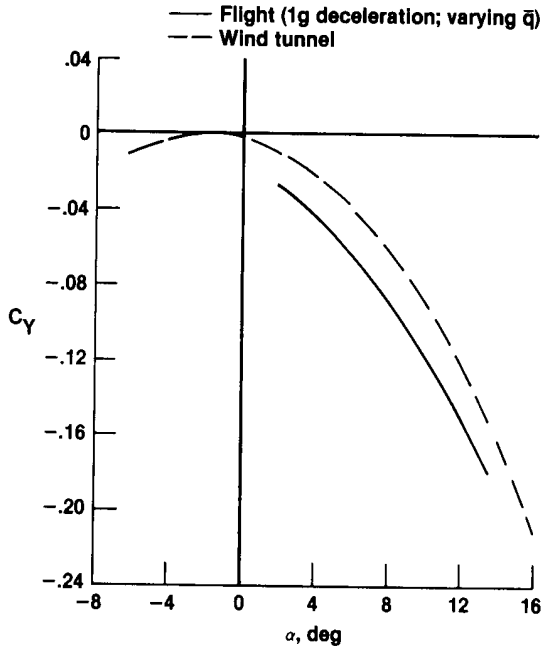

(c) Λ = 30°.

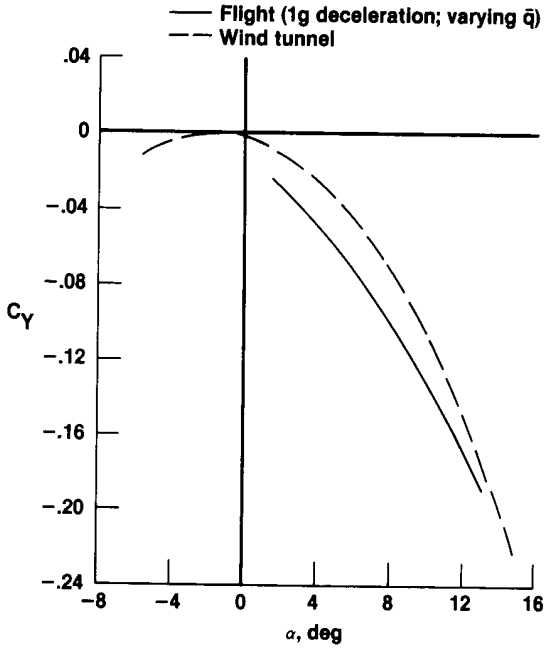

(d) Λ = 45°; 60°.

Figure 8. Concluded.

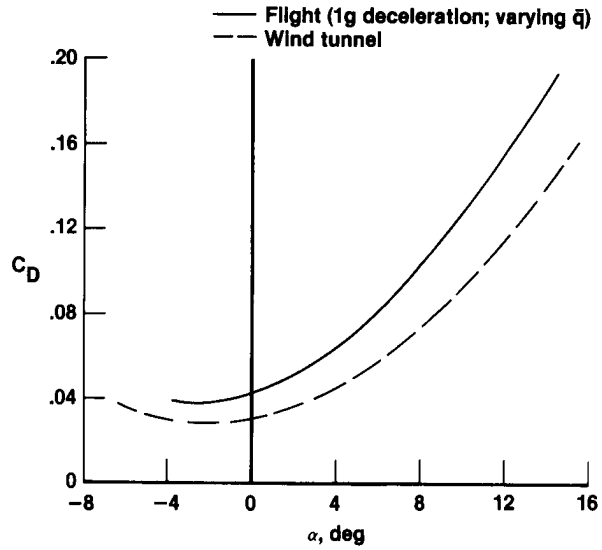

(a) $\Lambda = 0°$.

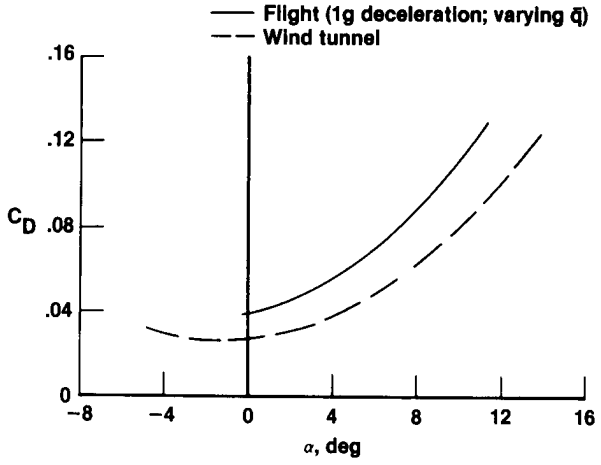

(c) $\Lambda = 30°$.

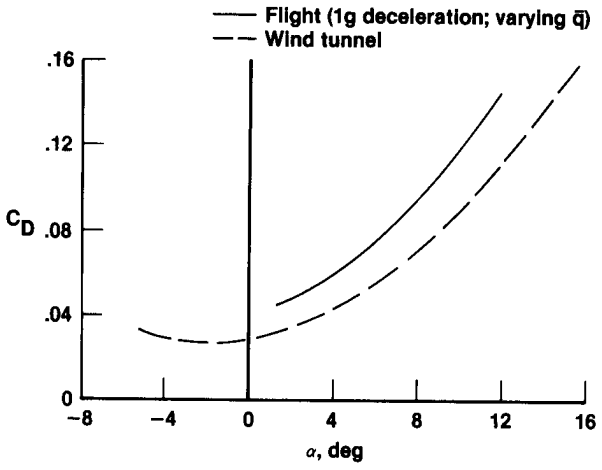

(b) $\Lambda = 15°$.

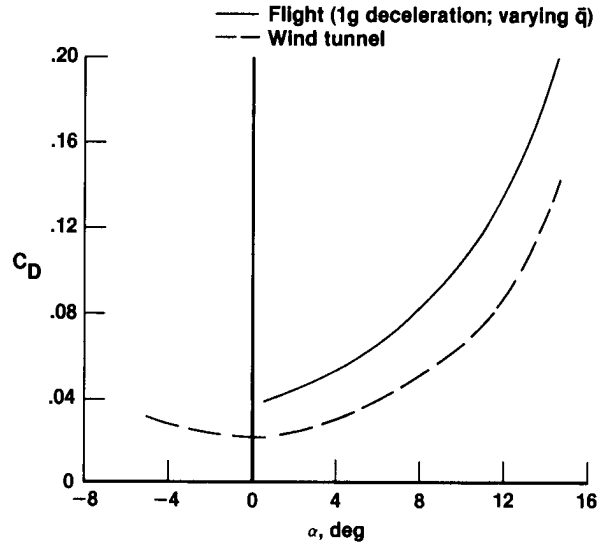

(d) $\Lambda = 45°$.

Figure 9. Untrimmed drag coefficient results.

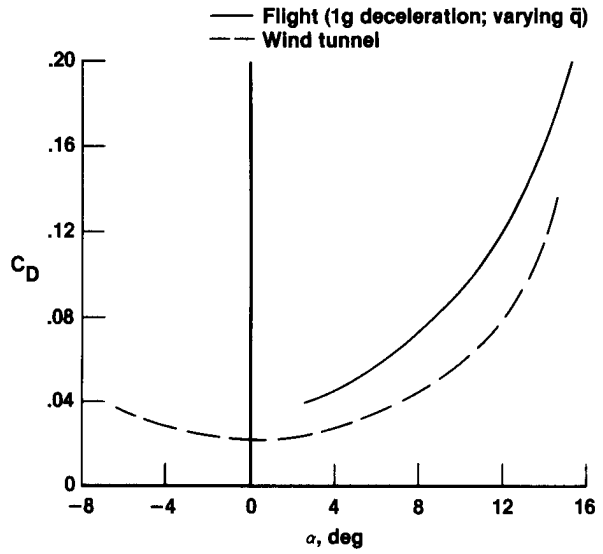

(e) $\Lambda = 60°$.

Figure 9. Concluded.

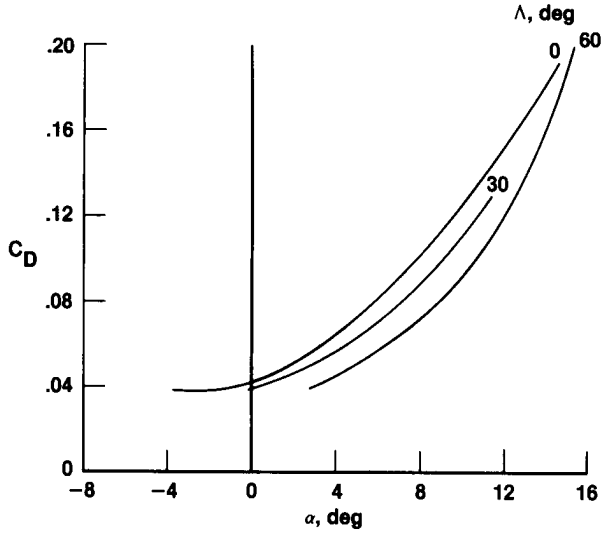

Figure 10. Flight data showing variation of drag with wing sweep; $\Lambda = 0°$, 30°, and 60°.

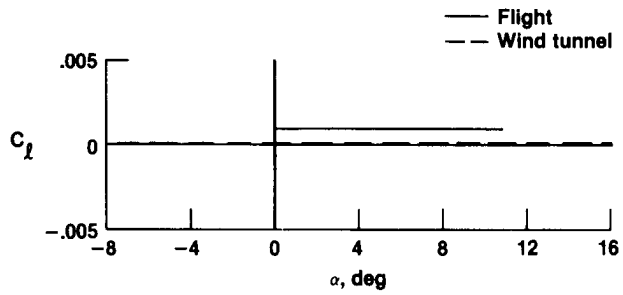

(a) $\Lambda = 0°$.

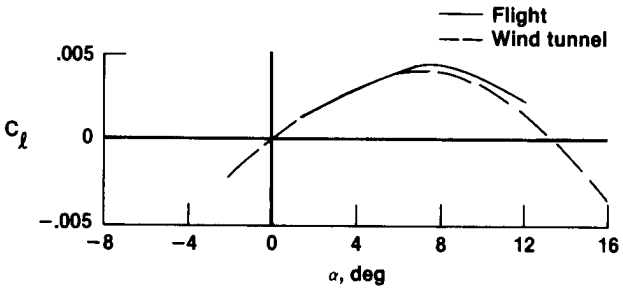

(b) $\Lambda = 15°$.

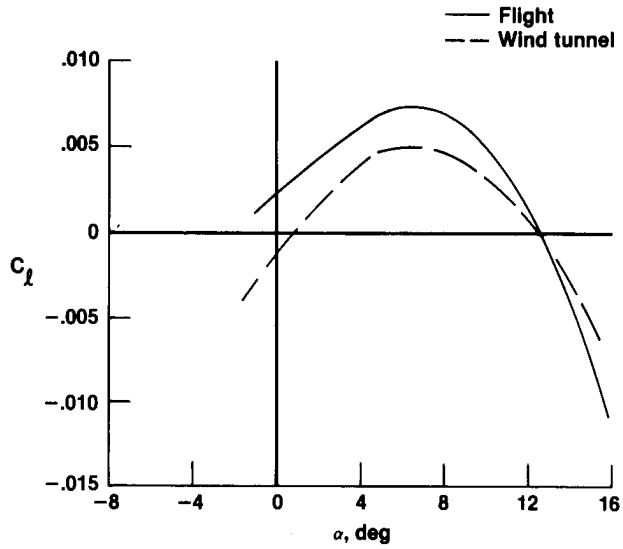

(c) $\Lambda = 30°$.

Figure 11. Untrimmed rolling moment coefficient results under 1g loading.

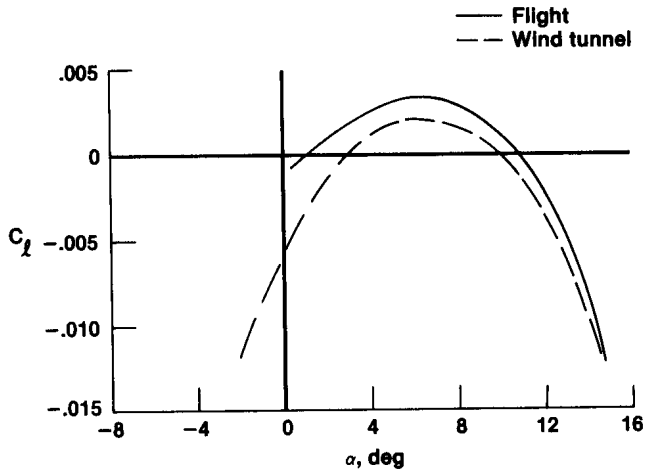

(d) Λ = 45°.

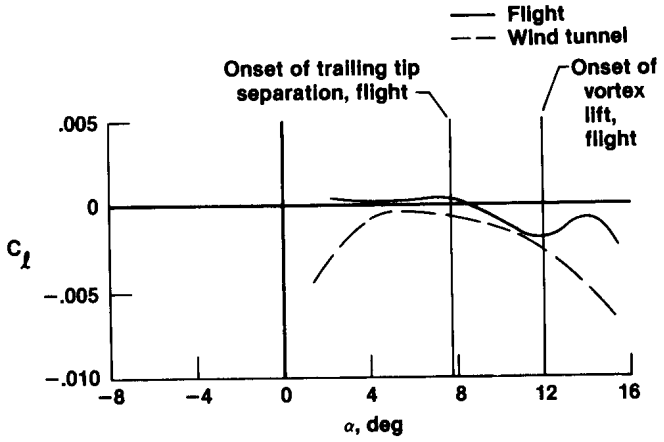

(e) Λ = 60°.

Figure 11. Concluded.

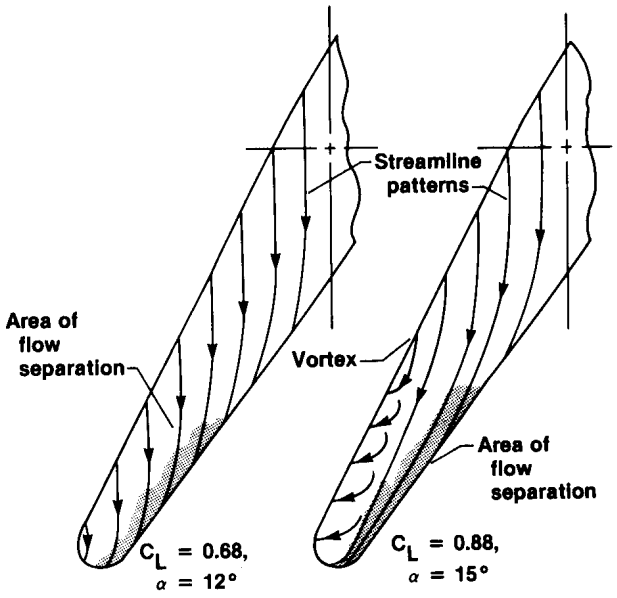

Figure 12. Trailing wing upper surface flow field; Λ = 60°.

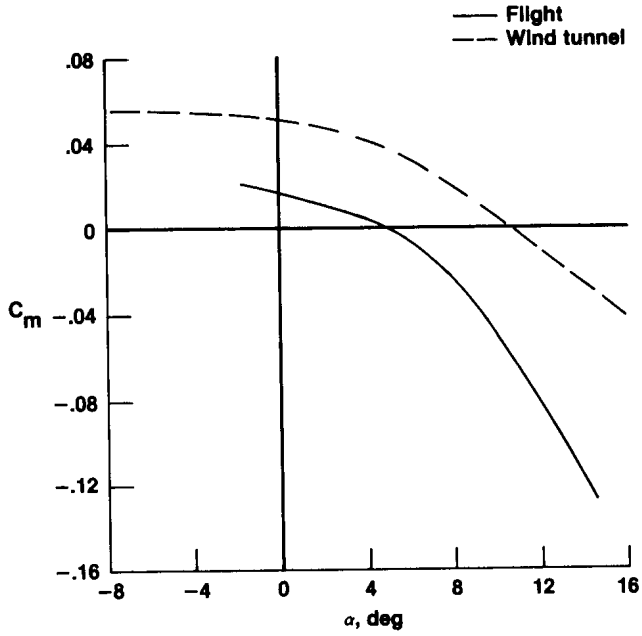

(a) Λ = 0°.

Figure 13. Untrimmed pitching moment coefficient results under 1g loading.

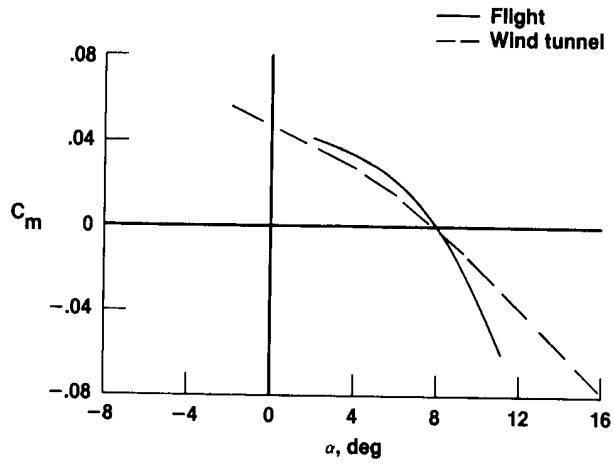

(b) $\Lambda = 15°$.

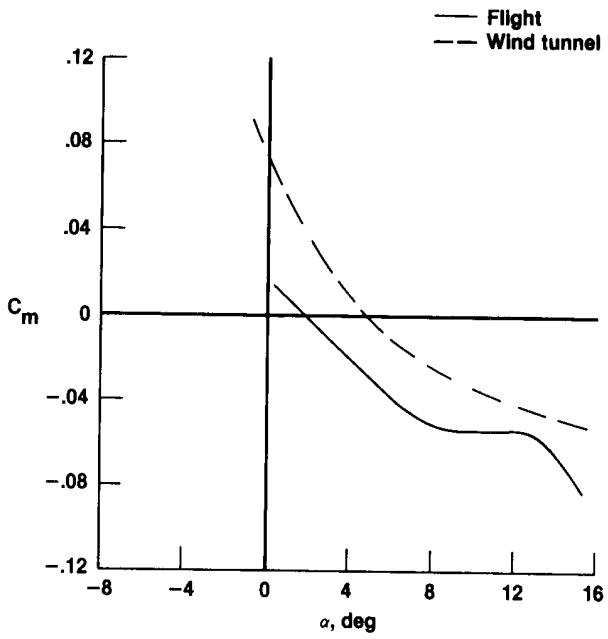

(d) $\Lambda = 45°$.

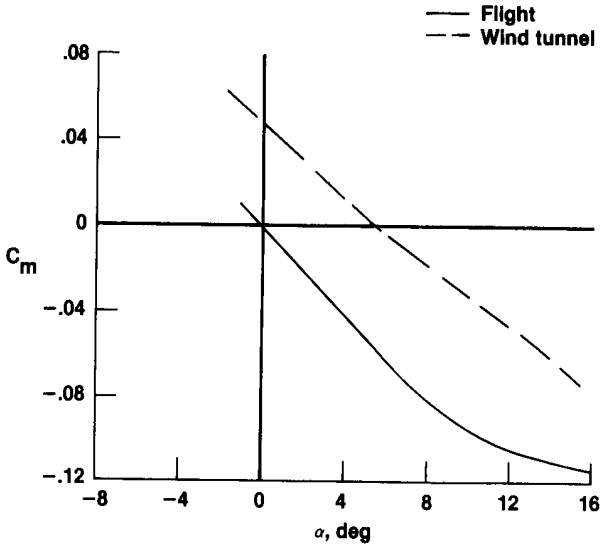

(c) $\Lambda = 30°$.

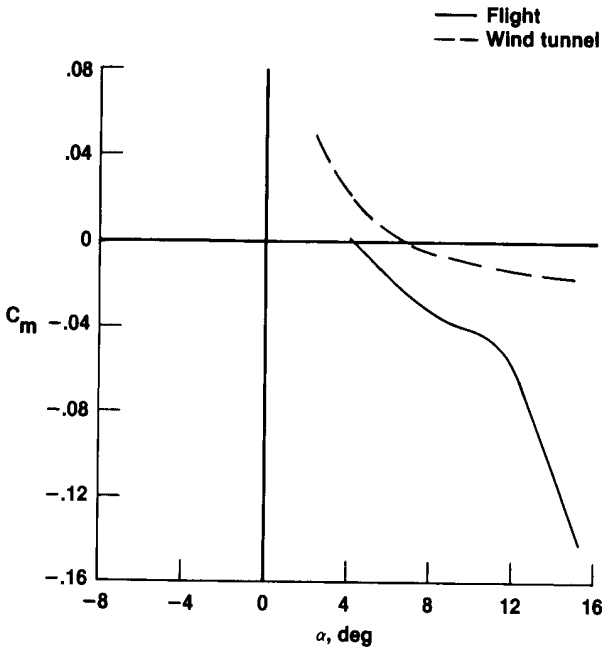

(e) $\Lambda = 60°$.

Figure 13. Concluded.

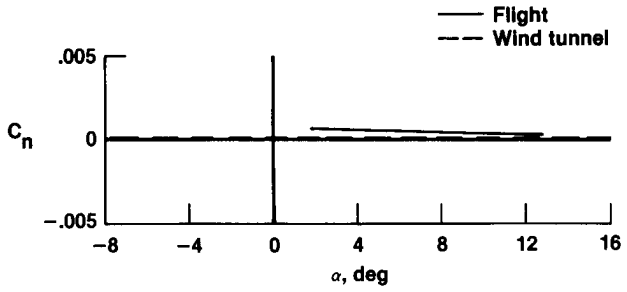

(a) Λ = 0°.

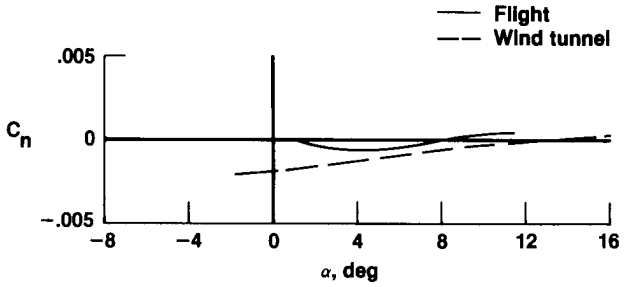

(b) Λ = 15°.

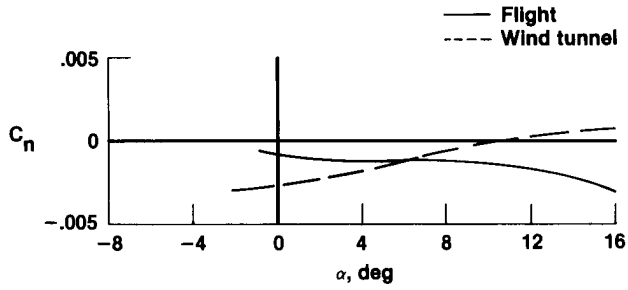

(c) Λ = 30°.

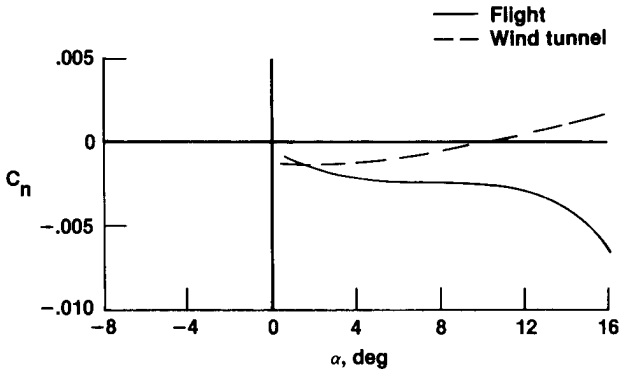

(d) Λ = 45°.

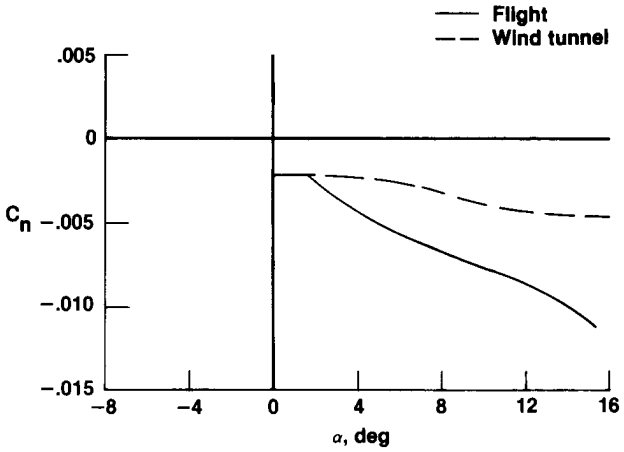

(e) Λ = 60°.

Figure 14. Untrimmed yawing moment coefficient results under 1g loading.

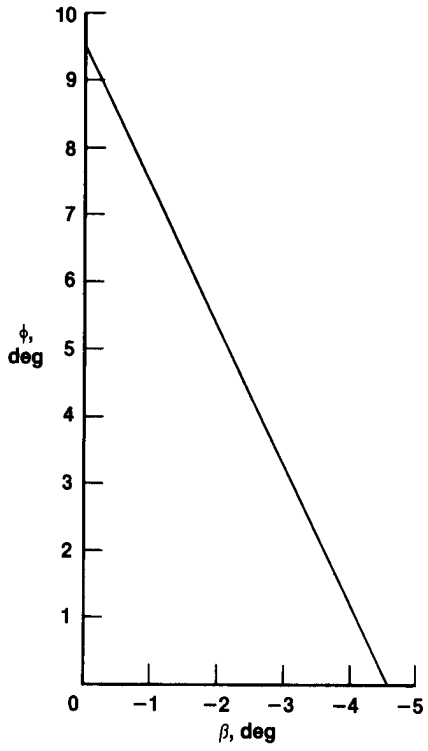

Figure 15. Flight estimates of the AD-1 airplane trim requirements at Λ = 60° and C_L = 0.3 and with right wing down.

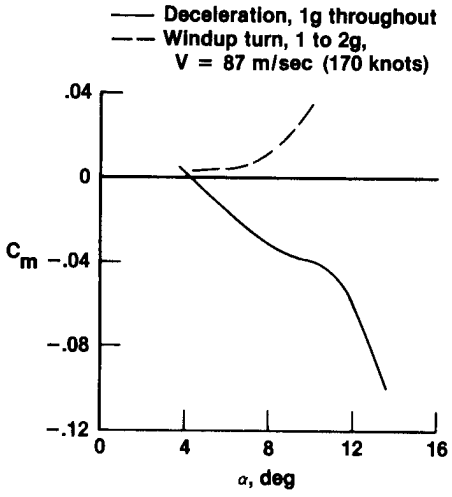

Figure 16. Example of load factor effects on the pitching moment coefficient; Λ = 60°.

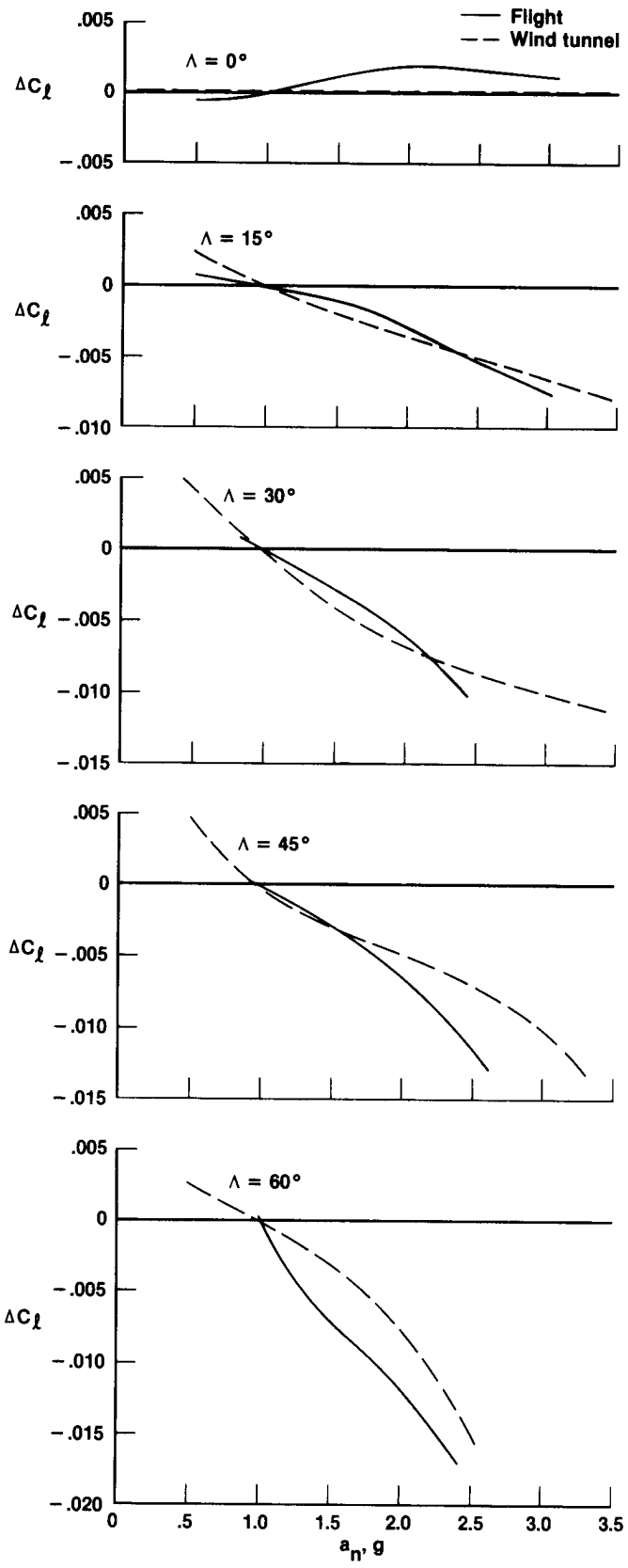

(a) ΔC_ℓ.

Figure 17. Incremental effect of load factor on moment coefficients at the design $\bar{q}$.

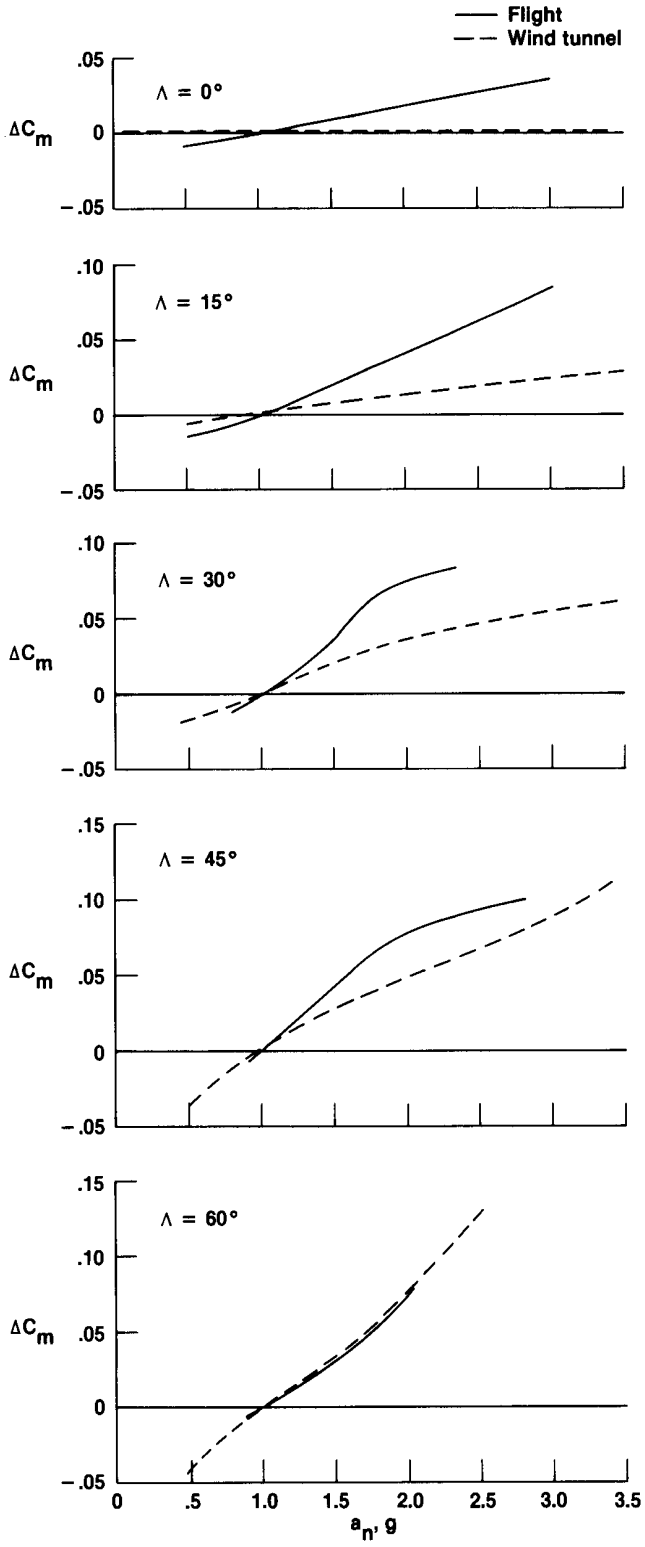

(b) ΔC_m.

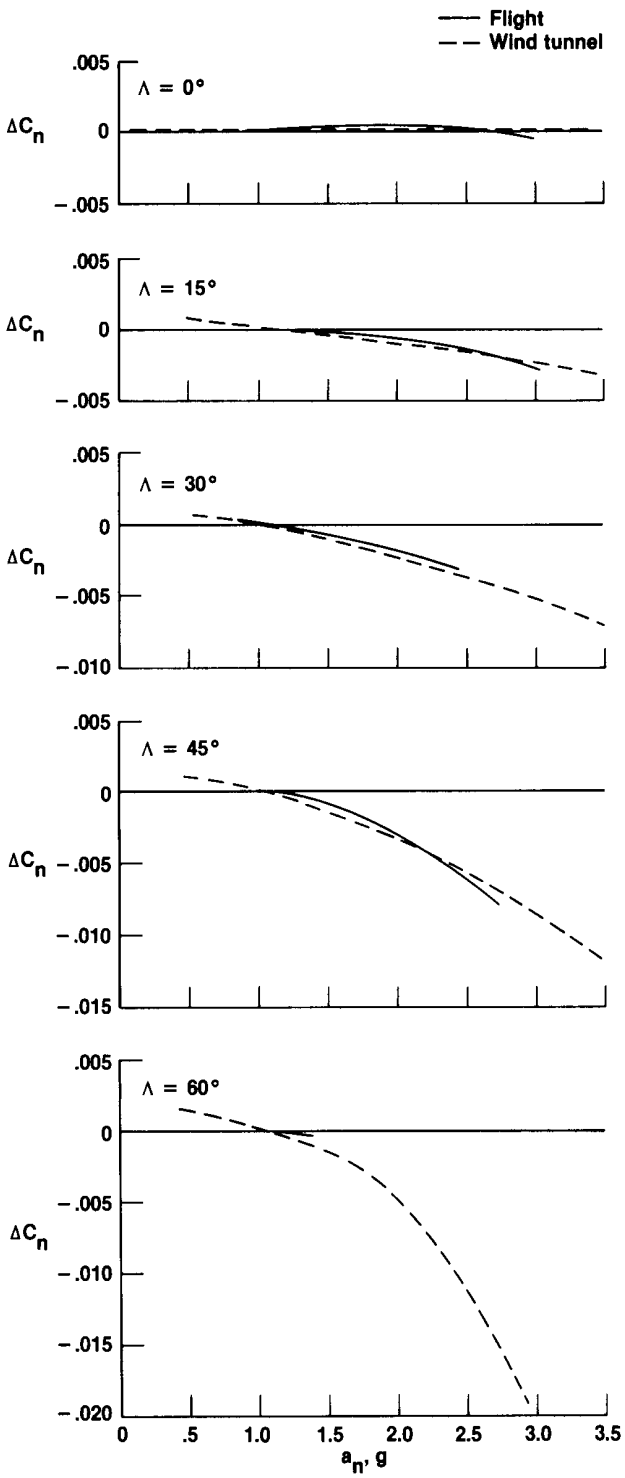

(c) ΔC_n.

Figure 17. Concluded.

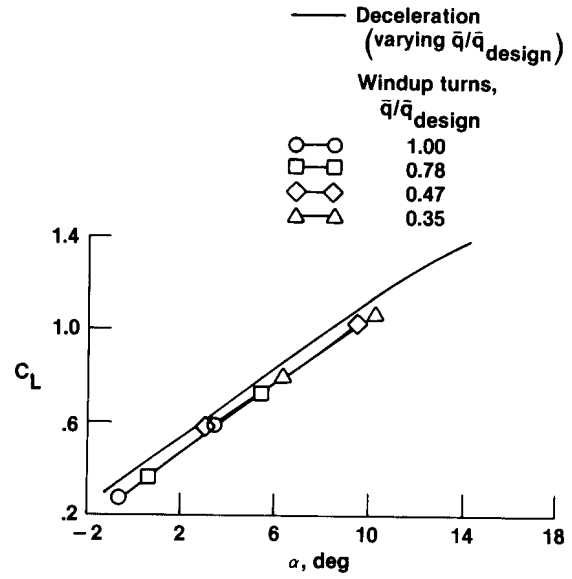

Figure 18. Comparison of lift coefficient from a deceleration and various windup turns; Λ = 35°.

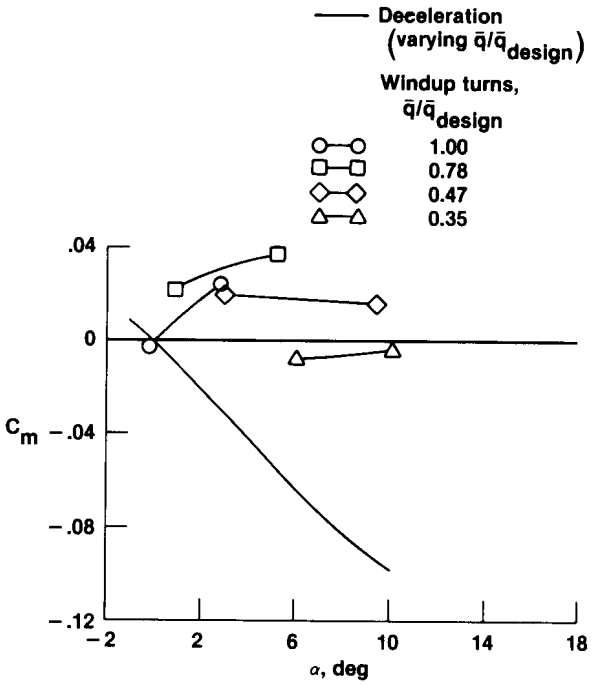

(b) Pitch coefficient.

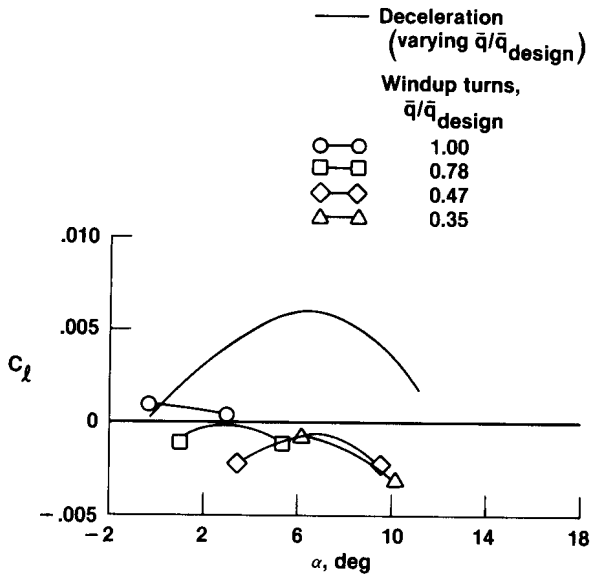

(a) Roll coefficient.

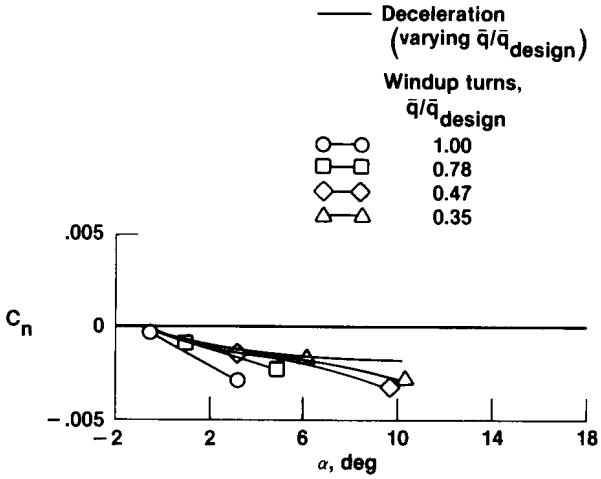

(c) Yaw coefficient.

Figure 19. Concluded.

Figure 19. Moment data from a deceleration maneuver (varying $\bar{q}/\bar{q}_{design}$) and windup turns at various $\bar{q}$ ratios; Λ = 35°.

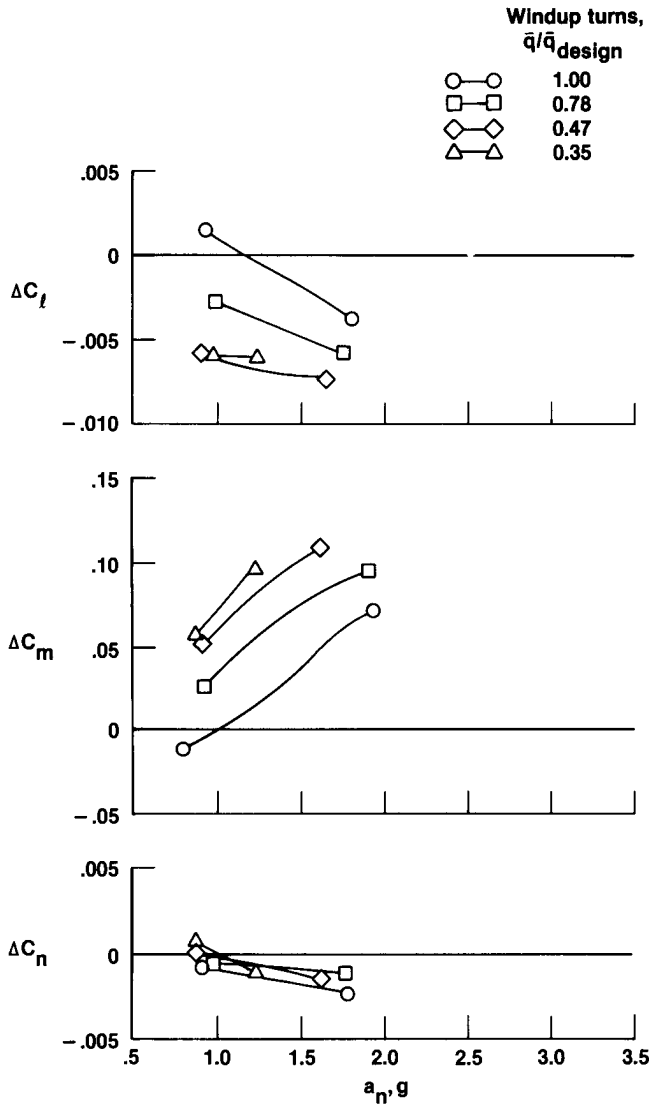

Figure 20. Moment increments at various $\bar{q}/\bar{q}_{design}$ ratios; Λ = 35°.

1. Report No.	2. Government Accession No.	3. Recipient's Catalog No.
NASA TP-2224		

4. Title and Subtitle	5. Report Date
In-Flight Total Forces, Moments, and Static Aeroelastic Characteristics of an Oblique-Wing Research Airplane	October 1984
	6. Performing Organization Code
7. Author(s)	8. Performing Organization Report No.
Robert E. Curry and Alex G. Sim	H-1181
	10. Work Unit No.
9. Performing Organization Name and Address	
NASA Ames Research Center Dryden Flight Research Facility P.O. Box 273 Edwards, California 93523	11. Contract or Grant No.
	13. Type of Report and Period Covered
12. Sponsoring Agency Name and Address	Technical Paper
National Aeronautics and Space Administration Washington, D.C. 20546	14. Sponsoring Agency Code RTOP 505-43-44

15. Supplementary Notes

16. Abstract

A low-speed flight investigation has provided total force and moment coefficients and aeroelastic effects for the AD-1 oblique-wing research airplane. The results were interpreted and compared with predictions that were based on wind tunnel data. An assessment has been made of the aeroelastic wing bending design criteria. Lateral-directional trim requirements caused by asymmetry were determined. At angles of attack near stall, flow visualization indicated viscous flow separation and spanwise vortex flow. These effects were also apparent in the force and moment data.

17. Key Words (Suggested by Author(s))	18. Distribution Statement
Oblique wing AD-1 aircraft Aerodynamic forces and moments Aeroelasticity	FEDD Distribution STAR category 08

19. Security Classif. (of this report)	20. Security Classif. (of this page)	21. No. of Pages	22. Price
Unclassified	Unclassified	28	

Available through NASA's Industrial Applications Centers

NASA-Langley, 1984